Experimental Characterization of the Double Stage Hall Thruster ID-Hall by Retarding Potential Analyzer

José Senart
jose.senart@tecnico.ulisboa.pt

Instituto Superior Técnico, Lisboa, Portugal

May 2019

Abstract

In this document we present a first approach to the characterization of LAPLACE's DSHT concept, the ID-HALL. This study was done using a RPA mounted in a rotating arm inside a cylindrical vacuum chamber facing the thruster. An ideal DSHT should allow the user to separately control Thrust (T) and specific impulse (I_{sp}) by adjusting mass flow, ionization stage power and acceleration stage voltage. Mass flow and ionization stage power should control the thrust only whereas power to the acceleration stage should control the specific impulse alone without affecting the thrust. In the ID-HALL's case these parameters are Xenon mass flow ($\dot{m}$), RF power to the FMICP source (P_{RF}) and DC voltage applied between the anode and the cathode (V_{DC}). Due to limitation with pumping at the time of this experimental work and because most measurements were only taken for the central position, thrust and plume divergence were only estimated in two cases and for a fixed, very low mass flow of 0.59 mg/s.
Keywords: Electrical Propulsion, Double Stage Hall Thruster, Retarding Potential Analyzer, Ion Energy Distribution Function

1. Introduction

The SPT was first developed in Moscow, USSR by Alexey Morozov in his doctorate thesis [18]. There were two main ideas behind his work: the creation of a strong electric field in the plasma bulk, using a transverse magnetic field and the use of the magnetic field to focus the ion flow, knowing that with sufficiently low electron temperature, the magnetic field lines are also equipotential lines [14]. This resulted in the development of the first ever SPT, then called E-accelerator model E-1, a model able to achieve specific impulses in the $1000 - 1800$ s range [18]. Several analytic and experimental studies and later flight tests aboard the Meteor type satellites led to the development of the SPT-60 (1969-1977) in EDB "Fakel" [2] first flown in 1971.

In SPT the electric field arises from the application of a potential difference between an anode close to the back of the thruster channel and an emissive cathode right outside the channel as it will be more thoroughly discussed in section 2.1. These devices use a radial magnetic field close to the exhaust plane that will lower axial electron conductivity making it so that most of the potential drop concentrates on this region. The specific configuration of Electric and Magnetic fields felt in this plane will cause the electrons to $E \times H$ drift in the azimuthal direction. This net current is called Hall current and will be responsible for the the ionization of the neutral flow of propellant. This makes it so that the applied voltage between anode and cathode V_{dc} is the sole parameter responsible for both ionizing and accelerating the positive ions.

Lately, as to maintain competitiveness with gridded ion thrusters, the DS concept has been being investigated of which a non exhaustive review will be made. The DSHT concept aims at separating the ionization and acceleration in two separate staged with the objective of controlling thrust and specific impulse independently. Ideally, in a DSHT, the ionization would be totally controlled by tweaking neutral mass flow and the power there deposited (ionization stage) whereas acceleration would be controlled by the power deposited by the applied V_{dc} (acceleration stage).

Several attempts have been made of developing a working DSHT concept. Albeit mostly unsuccessful in demonstrating a DS behavior they provide useful insight and will now be briefly overviewed. This work will focus specifically on the ID-HALL [5]. The ID-HALL is the new DSHT concept designed and developed at LAPLACE that is going to be studied in this thesis.

1.1. Prominent DSHT Concepts

As it was mentioned in the previous chapter, the ID-HALL is not the only design attempting at the

DSHT behavior. In this section and before approaching the ID-HALL operation, a brief review of the existing DSHT concepts will be made. DSHTs can be divided in two categories regarding geometry: Concepts with ionization either inside or outside the thruster channel.

Surfacewave DSHET

In this design a cylindrical resonance cavity is set upstream of the thruster channel as can be seen in Figure 1.1(a). A 5.8 GHz microwave is injected in it through a waveguide on the side which then propagates into the channel through the quartz window. High plasma densities are attained as the wave propagates along the dielectric-plasma interface, i.e. in a surface-wave mode.

The thrust measurements showed that thrust and specific impulse were higher with microwave injection rather than without [15] and higher thrust efficiency was attained for the first case at low discharge voltage, showing that it was indeed possible to operate in a double stage regime. A very important characteristic of the SW-DSHT is that the ionization region occurred very close to the magnetic barrier which allows an efficient extraction of the ions avoiding collision with the walls.

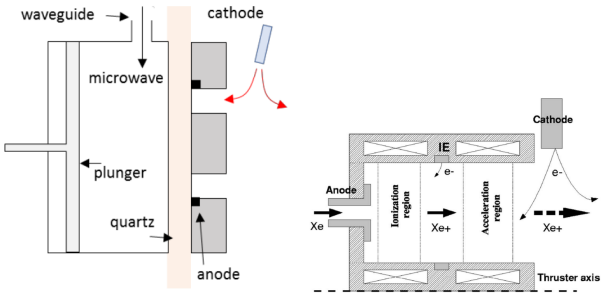

(a) (b)

Figure 1: DSHT with microwave ionization stage [5] (a). DSHT with intermediate electrode and four-coil configuration [20](b)

DSHET with Double Peaked-B Field & Intermediate Electrode

In the concept presented in Figure 1.1(b) the idea is to generate two separate magnetic barriers. The one upstream should act as the ionizing stage while the one near the exhaust should be the accelerating stage. This would be achieved making use of a third intermediate electrode between the two stages. The voltage applied between the intermediate electrode and the anode could then be controlled independently from the accelerating voltage. So far, it has been shown by simulations [20] that a non-negligible part of the ionization is occurring in the acceleration stage which would not correspond to a double stage operation.

Electron Bombardment Cusped DSHT NASA-173GT

This concept (Figure 1.1(a)) uses as ionization stage an electron bombardment plasma source. It's composed of an applied magnetic field that serves as magnetic insulation to prevent the ionization cathode's electrons from getting to the anode. Plume characterization and performance measurements [21] for both single and two-stage operations of the thruster showed two regimes provided approximately the same performance. There was no clear conclusion on wether an advantage in two-stage operation exists.

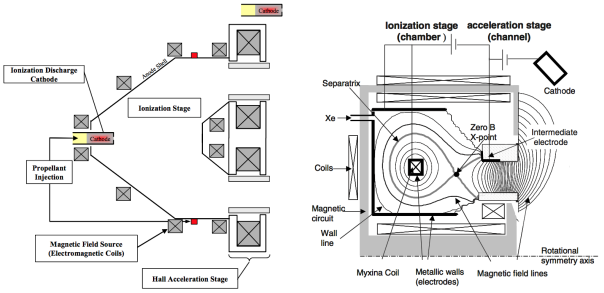

(a) (b)

Figure 2: Diagram of the NASA-173GT [21](a). Schematic of the SPT-MAG [12] (b).

SPT-MAG DSHT

The SPT-MAG concept, shown in Figure 1.1(b), was proposed by Morozov [19] and is based on a semi-galathea magnetic field design. This is applied as a form of magnetic confinement.

There is an intermediate anode that, while being the acceleration stage's anode, also serves as the cathode for the ionization stage. The special magnetic arrangement for this magnetic trap is generated by the magnetic circuit along with the coil at the center, called *Myxina*. In this configuration there is a zero B line intercepting the intermediate anode. This line is entirely at the intermediate anode potential because the B lines are equi-potential. In this configuration there is a potential drop from anode to this zero B line. This creates a potential well centered at this line where the ions get trapped and guided to the exit of the channel. The strong magnetic field in the voltage drop zone increases electron residence time creating a region of efficient ionization.

On the basis of the research of the SPT-MAG [7] it could not be concluded whether the thruster behaved as a DSHT as it was not clear if the electrons involved in the ionization were the ones heated in that stage or energetic electrons coming from the outmost cathode.

Electron Cyclotron Resonance DSHT

Figure 1.1(a) shows this concept where the ionization is done by applying a MW field with a frequency matching the electron cyclotron resonance frequency $\omega = eB/m_e$ [23]. There was however a

problem with this concept: In one hand there was an upper bound for ω. Higher frequencies would require stronger magnetic fields to maintain resonance which would in turn interact with the magnetic field of the magnetic barrier in the thruster channel. On the other hand, there is a critical cut-off density defined by $\omega = \omega_{pe}$ around 2.2×10^{11} cm^{-3} for a MW frequency of 4.25 GHz. This can not hold since optimal plasma density in hall thrusters should be higher than 10^{12} cm^{-3}. These two opposite end limitations kept the concept from being studied further.

Helicon DSHT

The last concept here presented is the one schematized in Figure 1.1(b) whose ionization stage consists of a Helicon source. These ion sources are able to produce plasma densities higher than the ones necessary for HT. As in the previous designs, no efficient operation in DSHT mode could be found. Experimental results have shown that thrust-to-power and total anode efficiency consistently decrease with increasing RF power [24]. Once again there were issues about the interaction of the magnetic fields involved in the ionization stage, and the radial magnetic field of the thruster channel magnetic barrier.

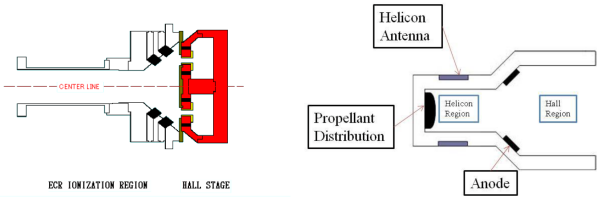

(a) (b)

Figure 3: ECR DSHT (a). Helicon thruster schematic side view[17](b)

1.1.1 Main Issues With the Previous DS Concepts

There are two main issues with the previously shown DS concepts. In a single stage Hall thruster atoms are ionized by electrons coming from the cathode. In a DSHT since the aim is to separate the stages, having ionization caused by cathode electrons accelerated in the intended region makes the DS operation seem futile since most of the ionization can be achieved by the acceleration stage.

It's intuitive to see that a thruster will not be efficient if it cannot accelerate the ions it produces. In fact, one of the reasons the classic HT is so efficient a source stems from the fact that the ionization and acceleration regions are overlapped. Seeing that DSHT attempts here presented consisted on basically attaching an ion source to the back of a typical single stage hall thruster one can understand that the distance between the these regions can constitute a problem. If ions are generated far away upstream, they have time to hit the channel walls and be annihilated before being extracted. For this reason, the ionization stage should be as close as possible or even inside the magnetic barrier.

2. Background

2.1. Theory of Hall Thrusters

A Hall Truster, contrary to its Gridded Ion Thrusters counter-parts, utilizes no potential grids to generate the accelerating Electric Field. As schematized in Figure 4 a HT's main structure consists of a cavity (for instance 2.5 cm length, $R_1 =$ 3.5 cm & $R_2 = 5$ cm inner and outer radius respectively for SPT100 [3]) bounded by cylindrical walls. The anode is placed near the propellant feed in the back while the cathode is placed outside the cavity next to the exhaust. A strong radial magnetic field on the order of a few 100s G is applied near the exhaust.

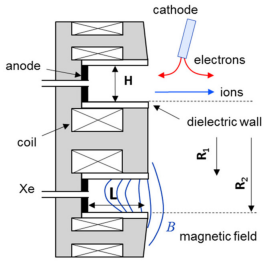

Figure 4: Scheme of a SPT.

During the operation of a HT, electrons leave the cathode towards the anode passing through a magnetized region close to the exhaust plane. To understand a fundamental aspect about how a HT works we must take into account the expression for the Larmor radius r_L for a particle with charge q and mass m, in a region submerged in the magnetic field B [8] $r_L = mv_\perp/|q|B$, where $v_\perp$ is the particle's speed perpendicular to the magnetic field. We can see that the much lower mass of an electron compared to that of an ion causes it to have a much smaller Larmor radius. The case of Xenon for instance, with an atomic weight of $M_{Xe} = 131$ amu and an exhaust velocity of 15 km/s yields $r_L \sim 2$ m. This means that, while the ions remain virtually unaffected by the B field, the electrons get trapped by this magnetic barrier, thus creating a zone of low electron conductivity. As to maintain current continuity $\vec{J} = \sigma\vec{E}$ a strong electric field arises. This electric field couples to the magnetic Field giving rise to a E×B drift in the electrons that according to the definition $\vec{v}_d = \frac{\vec{E}\times\vec{B}}{B^2}$ causes them to flow in the azimuthal direction. This drift current, designated Hall Current, will ionize the neutral flow coming from the anode side. The axial electric field will then accelerate the ions to extremely high veloc-

ities (typically a few tens of km/s [13]). After being accelerated, the ions will still be attracted by the high electron density in the magnetic barrier behind them. The electrons ejected out of the cathode will prevent this from happening, serving as a neutralizer by shielding them from this potential drop.

During the operation of the device, the anode will collect electron current coming from the channel. Ideally there would be no cathode current entering the channel and no ion losses to the walls and subsequent SEE so this value should correspond to the ionization current only. The total ionization current I_{full} is

$$I_{full} = \frac{e}{M_{Xe} \cdot m_{p^+}} \dot{m} \tag{1}$$

where M is the atomic weight of the propellant being used and m_p is the proton mass.

2.1.1 Thrust

Thrust is the force applied to the ship defined by the rate of change in its momentum [13]. It is equal to the rate of momentum exhausted in the propellant given by

$$T = \frac{d}{dt}(m_p v_{ex}) = \dot{m}_p v_{ex} \tag{2}$$

where, in the specific case of electric propulsion we consider only the ions ($m_{ex} = m_i$ and $v_{ex} = v_i$) since the contribution to the thrust from the neutrals is negligible due to their much lower exhaust speed. Equation 3 gives us the thrust considering only beam voltage V_b, beam current I_b, ionic mass m_i and ionic charge e for singly charged ions.

$$T = \sqrt{\frac{2m_i}{e}} I_b \sqrt{V_b} \tag{3}$$

2.1.2 Specific impulse

Specific impulse I_{sp} is by definition the ratio of thrust to consumption of propellant

$$I_{sp} = \frac{T}{\dot{m}_i g} \tag{4}$$

where g is the acceleration of gravity at earth's surface 9.807 m/s^2. Just by looking at equation 2 it is clear that I_{sp} is a quantity equivalent to the exhaust velocity

$$I_{sp} = \frac{v_{ex}}{g} \tag{5}$$

Specific impulse can be thought of as the time it takes to run out of 1 kg of propellant while providing 9.8 N of thrust.

2.2. ID-HALL

The design presented in Figure 5 is a prototype that aims at studying the basic physics of the thruster.

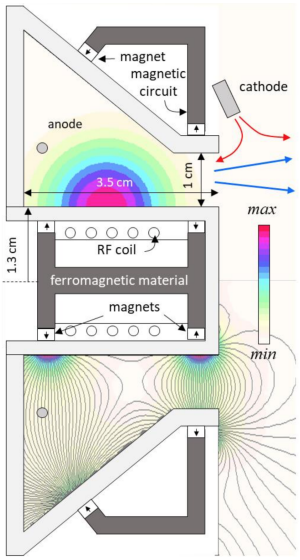

Figure 5: The ID-HALL Double-Stage Hall Thruster. The inner cylinder is made of quartz and the other walls in the ionization chamber and in the channel are made of ceramic material. The 2D plots represent the magnetic field distribution (bottom; color plot: field intensity, lines: magnetic field lines) and the assumed spatial distribution of the power absorbed per electron, $\Theta_{RF}(x, r)$ (top)[10].

2.2.1 Ionization Stage

In the ID-HALL, the ionization stage consists of a ICP source in the inner cylinder of the HT. When a time-varying current passes through the coil it creates an axial magnetic field. Since this magnetic field is time-varying as well, it in turn induces an electric field that, according to Faraday's law of induction

$$\nabla \times \vec{E} = -\frac{\partial \vec{B}}{\partial t}, \tag{6}$$

is in the azimuthal direction. This way the electrons traveling back and forward along the magnetic field lines get heated by the electric field and the gas becomes ionized.

The source used on the ID-HALL is what is known as a FMICP. It was shown that the use of a permanent magnet inside an ICP source can significantly increase electron density and decrease electron temperature due to the confinement provided by the permanent magnetic field [25, 1, 9]. These sources generate a well localized toroidal plasma that can achieve densities on the order of a few 10^{11} cm^{-3} [9].

These are values similar to the ones achieved in the ECR concept but in that case it was not possible to increase as there was a critical density. The values stated here were for the IC source alone, and

they are expected to increase in the magnetic configuration provided by the ID-HALL DSHT. Furthermore, the axisymmetric geometry of the source is especially well suited to the integration in the interior of a HT. At last, because of how they are shaped, it allows testing of different configurations with readjustments in the axial position.

Note that in order to confine the plasma, limiting losses to the walls, the magnetic circuit is designed as to generating a magnetic field with components parallel to the walls. This implies the magnetic cusps shown in Figure 5. This magnetic field configuration also has not one but two magnetic barriers as it can also be seen in the bottom half of Figure 5. The first one is the necessary one for a HT in the exhaust region and the second one is located close to the backplate, directly crossing the anode.

2.2.2 Computational Model

Leading to the prototyping of the device we are studying in this thesis a computational model was used to simulate the design. The HALLIS software, a hybrid fluid-particle simulation model developed by Prof. Jean Pierre Boeuf [16] was used to go about these simulations. This is a quasi-neutral 2D model in the radial-axial plane where ions are treated as particles whereas electrons meet a fluid treatment. Since collisional electron mobility is not sufficient to explain observed cross-field transport, in this model electron mobility is described using effective collision frequencies that depend on adjustable (anomalous transport) coefficients. A more detailed description of the model can be found in [10], where the ID-HALL concept was first proposed.

Simulation Results

It is now important to mention some simulation results that will be taken as reference in the upcoming data analysis. In a single stage the operation was led with an applied voltage of $V_{DC} = 250$ V and a mass flow rate of 2 mg/s. It should be noted that there are no low frequency oscillations (or breathing mode) in these conditions. In these conditions the simulation ran as expected from a classic SPT. Though the value of electron current flowing into the channel is strongly dependent on the anomalous transport coefficients, for a taken fixed value of these coefficients, a total discharge current of 1.98 A was obtained. The current corresponding to full ionization of 2 mg/s of singly ionized particles is 1.47 A which leaves 0.51 A of current that is entering the channel. The calculated ion beam current is 1.38 A that yields a 94% ionization rate and a total of 0.6 A of cathode current entering the channel [10].

The position of the anode was shown to influence the plasma properties. Figure 6 shows that for the situation when the anode is closer to the back plate (3mm) there are two steps in the potential.

That first step stems from the fact that at that position, the anode is behind the second magnetic barrier, visible on the magnetic landscape in the lower half of Figure 5. The anode is represented with a gray dot positioned 3mm from the back plate. In order to maintain current continuity the electric field has to be higher in that region, giving rise to a change in potential. When the power source is turned on at 100W we can see that the step disappears for the same position of the anode. This is because the high plasma densities imposed by the ionization stage increases the electron conductivity hence making the necessary electric field be lower or even 0.

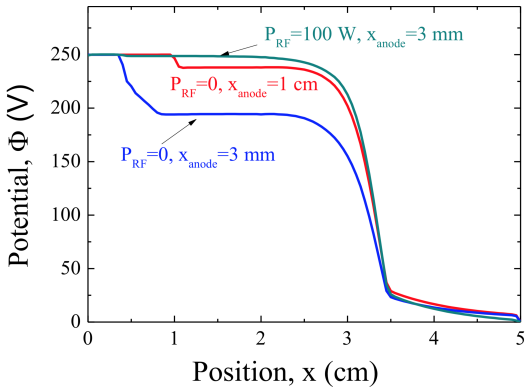

Figure 6: Axial profiles of the electric potential along the middle of the channel, for $V_{DC} = 250$V and for 3 conditions: no RF power and anode at 1 cm from the back plate, no RF power and anode at 3 mm from the back plate, and $P_{RF} = 100$ W and anode at 3 mm (image and caption from [10])

2.3. Diagnostics

2.3.1 Retarding Potential Analyzer

The operation of a RPA is rather simple and straight forward. It is composed of 4 grids and a collector plate. The grids have different purposes that are as follows:

The first grid G_0 is just a screen grid. It is there to shield the plasma from the effects of the others grids's potentials. To do this it has been grounded and no other potential was ever applied to it.

Since the objective is to draw an ion distribution, only ions should be filtered and collected in the interior of the RPA. Having that in mind an electron rejecting grid G_r is held at a high negative potential after the screen grid.

The third and next grid G_a is where the ion filtering is done. A sweep voltage is applied here ranging from 0 to high positive potentials. The idea is simple: the higher this voltage is, the smaller the current collected in the bottom plate should be, as it is rejecting more and more energetic ions at each step.

The last (and usually considered optional) grid G_{ad} has the job of dealing with SEE. When ions hit the collector plate there is a probability that a secondary electron will be emitted. If this happens then this ion will be erroneously counted twice. By holding this last grid at a fairly high negative potential one can bounce these SEE back to the collector, thus avoiding double counting.

Ion Energy and Velocity Distribution Functions

Following the procedure in [22], the method for extrapolation of meaningful physical quantities from the RPA data is presented in the full text. It can be shown that, when running an RPA, the IEDFs and IVDFs can be extracted using the expressions

$$\begin{aligned} f(v_x) &= -\frac{m}{q^2 A\tau}\frac{dI_c}{dV}\bigg|_{V=V_a}, \\ g(E_x) &= \frac{1}{q^2 A\tau}\sqrt{\frac{m}{2qV_a}}\frac{dI_c}{dV}\bigg|_{V=V_a}, \end{aligned} \tag{7}$$

where I_c is the collector current, m and q are the ionic mass and charge respectively, A is the collector area, τ is the transmittance and V_a is the sweep voltage.

Specific Impulse and Thrust

Specific impulse was seen in Equation 5 to be a quantity equivalent to v_{ex}. Experimentally, v_{ex} is calculated taking its expected value in the measured IVDF, v_{avg}

$$v_{avg} = \frac{\sum_{v=v_{min}}^{v_{max}} v \cdot f(v)}{\sum_{v=v_{min}}^{v_{max}} f(v)} \tag{8}$$

Thrust can also be put in rather simple terms and can be calculated using 2. What we can access with the RPA though is $J * \tau$, the current density at a specific position so what we get is a thrust per unit area $t = J_b v_{avg}\frac{m_{ion}}{q_{ion}}$.

$$t = \dot{m}_i v_{avg} = J_b v_{avg}\frac{m_{ion}}{q_{ion}} \tag{9}$$

Both J and v_{avg} are actually dependant on the angle regarding the center of the thruster, $J \equiv J(\theta,\phi)$ and $v \equiv v(\theta,\phi)$. Therefore t and I_{sp} will also be functions of θ and ϕ. To obtain the final value T in section we will have to integrate $t(\theta,\phi)$

$$T = \int_0^{2\pi}\int_0^{\theta_{max}} R^2 sin(\theta) t(\theta,\phi) d\theta d\phi \tag{10}$$

Plume Divergence

As to compare the beam profiles looked into in section 3 we will also need to estimate plume divergence. Since v_{avg} doesn't vary with angle we can use [6]

$$< cos(\theta) >= \frac{\int_0^{\pi/2} J_b(\theta) cos(\theta) sin(\theta) d\theta}{\int_0^{\pi/2} J(\theta) sin(\theta) d\theta} \tag{11}$$

where the angle of the particles regarding the center axis is averaged over the plume, yielding a divergence angle λ.

$$\lambda = cos^{-1}(< cos(\theta) >) = cos^{-1}(\frac{I_{ax}}{I_b}), \tag{12}$$

where I_{ax} is the axial component of the current.

Coupled RF and DC Powers

We will calculate the coupled ICP power P_{RF} using the expression

$$P_{RF} = P_{inj} - \frac{1}{2}R_{coil}I_{coil}^2, \tag{13}$$

where R_{coil} is the resistance of the coil that at that frequency was measured to be 3.14Ω and I_{coil} is the measured current amplitude. The power injected via application of discharge voltage V_{DC} can be estimated using:

$$P_{DC} = V_{DC} I_d \tag{14}$$

3. Results

The arm upon which the RPA was fixed is able to rotate about an axis allowing a sweep between a maximum angle of $\theta = 21^o$ as see from the thruster to each side as it is shown in figure 7.

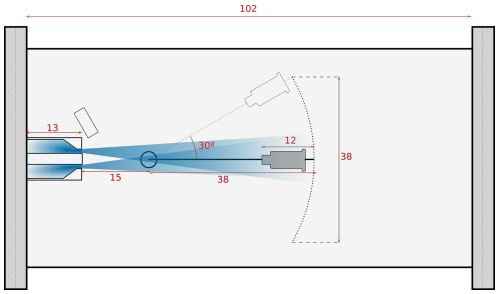

Figure 7: Scheme of the vacuum chamber with rotating arm mounted. All quantities in the scheme are expressed in cm.

The angular profile was taken with 6^o intervals for two distinct cases of applied power $P_{RF} = 0$ W and 100W with $V_{DC} = 100$ V. The distributions for these two sweeps are plotted in figure 8. Looking at these profiles we can immediately see that the single stage IEDF have two peaks whereas the double stage distributions have only one. We can also see that the beam angular spread of the distributions is different. In single stage, the peak lowest in energy has a bigger divergence than the most energetic.

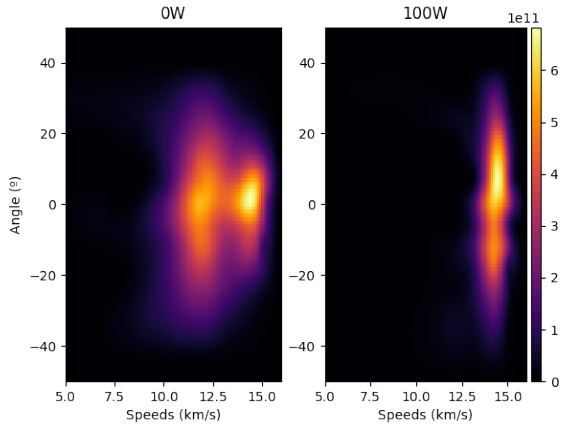

Figure 8: RBF interpolation of the IVDF taken for all the angles for $P_{RF} = 0$ W (left) and $P_{RF} = 1000$ W (right).

The peak we see in double stage in more divergent as well ranging to angles close to 40^o.

Angle measurements were taken also with the purpose of estimating thrust and specific impulse. For that to be possible we needed to build a surface of the thrust pressure $t(\theta, \phi)$ (eq. 9) in the spherical cap covered by the RPA. This surface must then be integrated using equation 10 to yield the total thrust. If we take $\phi = 360^o, 0^o$ for values with $\theta > 0$ and $\phi = 180^o$ for $\theta < 0$ we get a grid of currents that we can interpolate, giving rise to the surface seen in figure 9 for the spherical cap. The estimate values attained by this method are presented in table **??**.

Table 1: Comparison of performance metrics for both cases single-stage and double-stage with applied RF power of 100W. We used the Faraday probe scaling factors obtained directly from measurements for 150V and for 0W and 100W respectively.

	0 W	100 W
P_{RF} (W)	0.00	83.1 ± 0.6
P_{DC} (W)	150.0 ± 0.9	99.8 ± 0.6
I_b (A)	0.065 ± 0.023	0.080 ± 0.028
E_b (eV)	106.1 ± 0.2	132.8 ± 0.2
$Thrust$ (mN)	1.2 ± 0.5	1.8 ± 0.7
λ (^{o})	28.0 ± 2.1	31.5 ± 2.4

3.1. Single Stage

For this study the thruster was run without RF power applied to the coil. The DC voltage applied between the anode and the cathode V_{DC} was varied from the minimum possible value at which the plasma could be sustained to 200V. The distributions are plotted in figure 10(a).

It is clear from the figure that a double peak behaviour is present throughout all the distributions as it was in figure 8. The average ion energy was calculated and is plotted as a function of the applied voltage V_{DC} in Figure 11. It increases linearly with V_{DC} as was to be expected from a typical single stage hall thruster.

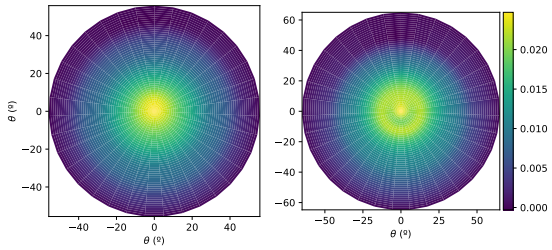

Figure 9: Estimation of the pressures exerted by the plume front in the spherical cap covered by the RPA.

3.2. Double Stage

The voltage applied between the anode and the cathode was swept from the minimum possible operating voltage up to 200V having fixated the RF power at 4 different values. The Anode-Cathode Voltage V_{DC} is the parameter used to control the average speed which ions will be accelerated to.

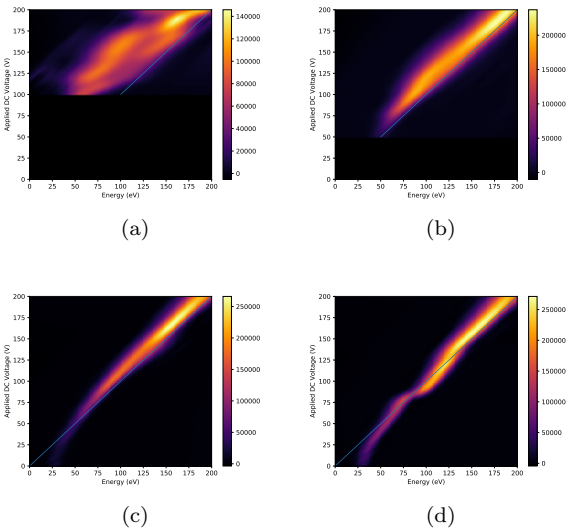

(a) (b)

(c) (d)

Figure 10: Distributions for the tension sweeps done for four different applied RF powers 0W, 50W, 100W and 150W. The line $E_b = V_{DC}$ is plotted for comparison.

The distributions are plotted in Figure 10. There we can se an increase in magnitude and peak energy

with increasing V_{DC} that can also be seen in Figure 11. As the applied power increases we start seeing narrower distributions as well.

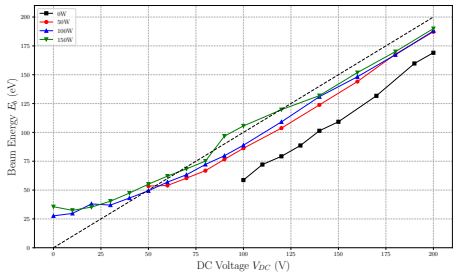

Figure 11: Measured average beam energy E_b for the tension sweeps for each of the four selected $V_{DC}s$ 0W, 50W, 100W and 150W.

When looking at figure 11 we can distinguishing two regions where the behaviour is different. After around $V_{DC} = 80V$ the increase is linear but before that value we see the curves tending to a constant value.

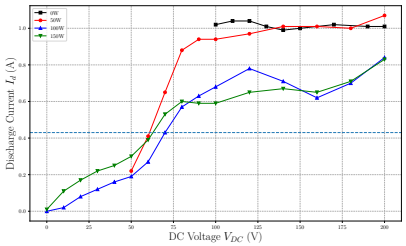

Figure 12: [Discharge current - black line indicates the ideal full ionization current for 6 sccm of Xenon, 0.43 A.

Discharge current I_d is plotted in Figure 12(a) alongside it's oscillation frequencies in 12(b). We that in all cases the discharge current tends to a plateau above $V_{DC} = 75$ V. Before this plateau and for the values of V_{DC} that could not hold the plasma with $P_{RF} = 0$ W we see an increase of I_d with V_{DC}. The oscillations exist only for the cases of $P_{RF} = 0$ W and 50 W. Their frequencies clearly increase with V_{DC} of $P_{RF} = 0$ W but not for $P_{RF} = 50$ W, where they are roughly constant.

The converse of the previous procedure was then carried out: for different fixed values of the applied DC voltage V_{DC} we swept the injected RF power from the minimum possible operating values to a maximum of 200W injected RF power.

All the distributions are plotted in figure 13 along with the line $E = qV_{DC}$ again as it was in figure 10. We can see now that, where we saw an increase

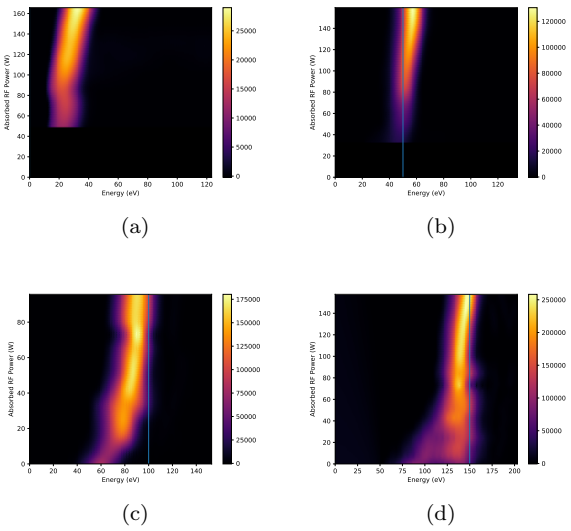

Figure 13: Distributions for the power sweeps led using V_{DC} =0V, 50V, 100V and 150V. The line $E_b = qV_{DC}$ is also plotted for comparison.

in peak energy when V_{DC} was swept, we now see a roughly constant value in the power sweeps, again in accordance with the reference $E = V_{DC}$ line as it is also clear in Figure 14. Again there are two regimes that were seen in Figures 10 and 11. In the first, for $V_{DC} = 0$ V and 50 V, $E_b > qV_{DC}$, the second in for then remaining, higher voltages where E_b remains bellow V_{DC} but approaches it with increasing P_{RF}. The distributions are also becoming wider with higher V_{DC} and in each P_{RF} sweep we see them getting narrower with increased P_{RF}.

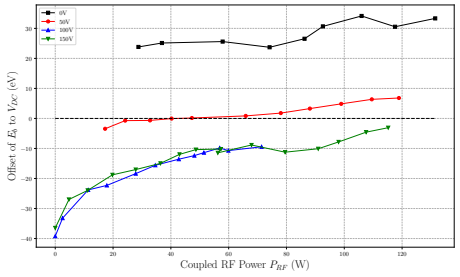

Figure 14: Difference of the average beam energy E_b to the applied V_{DC} for the power sweeps for 0 V, 50 V, 100 V and 150 V .

During the course of experiment we noticed that there were oscillations in the discharge current in the KHz range. These oscillations were not present when higher ICP powers were applied but at very low powers we could still observe them. We swept the injected power from 0W to 10W and plotted the resulting frequencies (fig 16). We can see that oscil-

lations disappear for specific RF powers and, looking at their corresponding distributions in Figure 15 we see that these correspond to the narrowest distributions.

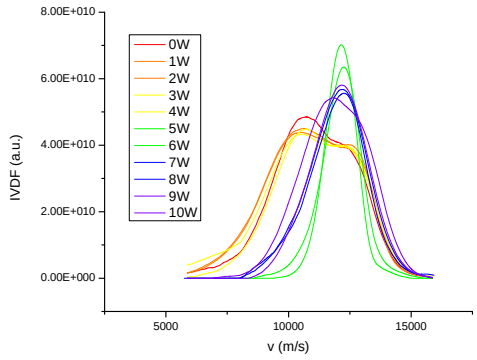

Figure 15: IVDF for the low power range of the P_{RF} sweeps.

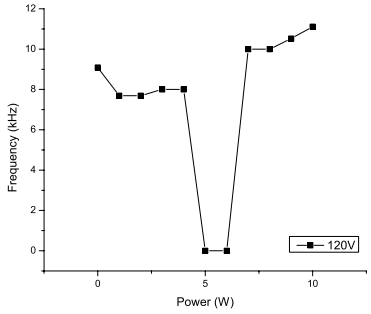

Figure 16: Frequency of discharge current oscillations in the low power range of the P_{RF} sweeps.

3.3. Discussion

We should first looking at the tension sweeps of Figure 10. In the ideal case, we would expect that the beam energy E_b was equal to the accelerating voltage. That's not the case but we can see that E_b increases linearly with V_{DC} for all the applied RF powers and single-stage alike. If we look at Figure 11 though, an effect of the applied RF power becomes evident - application of increased P_{RF} allowed for operation of the thruster at lower V_{DC}s. If we can sustain the plasma using the FMICP source at voltages where we would otherwise fail to do so, it must mean that part of the ionization power is being provided by the ionization stage. As we mentioned the behaviour is not exactly linear, namely in the low V_{DC} region ($V_{DC} < 80$ V), the measured E_b is higher than than V_{DC}. Similarly, in Figure 14 the voltages for which the plasma would not hold in single stage, 0V and 50V, E_b went above the applied V_{DC}. That is because the peak we measure corresponds in essence to the plasma potential at its origin where the positive ions started their acceleration. It's clear then that if we generate an ICP plasma, V_p at its core won't be zero so ions will still accelerate outwards and exit the thruster channel regardless of the fact that no accelerating voltage has been applied. In these low voltages we can say that the ionization stage is playing a role in the acceleration of the ions even if just by diffusion, which is as undesirable as the opposite case.

We can again take a look at the discharge current measurements in Figure 12. Two different regimes can be seen here again, separating values for which V_{DC} is not able to sustain the plasma by itself 0 V and 50 V from the other two. When increasing V_{DC} with fixed P_{RF} we see that I_d grows until it hits a plateau. This value is very much above the full ionization current $I_{full} = 0.43$ A reaching values of $I_d = 1$ A. This shows that there are other current sources other than the ionized flow as we have seen before such as SEE in the channel walls and cathode electrons being carried by anomalous transport off the magnetic barrier. This value does decrease greatly when higher ionization stage powers are applied. Now looking at the P_{RF} sweeps, for the two lowest voltages I_d increases with P_{RF}, approaching the full ionization current of 0.43A. This indicates higher ionization since the increasing number of electrons striped from the neutral flow will be collected in the anode. On the other hand, I_D decreases in the cases of 100W and 150W, which means less power is being provided by the V_{DC}. This could just mean that V_{DC} is providing less energy to the acceleration stage but as we can see in Figure 14 the average beam energy is non-decreasing, which means that the power provided to the acceleration stage is non-decreasing as well that in turn leaves the conclusion that the ionizing contribution from V_{DC} decreases. This reduction in DC ionization results in a smaller flux of cathode ions into the channel, lowering I_D. In the case of 0V applied all we are measuring is the distribution generated by the ICP but centered in the plasma potential. Each particle inside the channel will accelerate to the RPA going down the slope from V_{Pl} to 0 without the need for the application of an accelerating voltage.

In both 100 V and 150 V cases (Figure 14) we have seen a behaviour congruent with the simulation results. For lower powers, the average energy of the beam is lower indicating a smaller potential step at the magnetic barrier downstream from the ionization stage. When we increase the applied RF power, the beam average energy increases in accordance with the increase of the potential step on the

exhaust region observed in figure 6.

3.3.1 Anode Current Oscillations

The existence of two peaks in the single stage distributions (Figure 10(a)) shows the existence of two different populations of ions. One, corresponding to the highest in energy, is always the beam. After analyzing the frequency behaviour in the graph of Figure 16 and the respective distributions in Figure 15, we can see that the cases for which no oscillations occur coincide with the single peak distributions, lowest in FWHM. Remember that, as seen in section 2.3.1, the coupled DC power can be calculated using the discharge current meaning that an oscillation in the current implies an oscillation in the coupled power and effective applied electric field. Having said that we can conclude that the double-peaked distributions are a result of an oscillation in the supplied DC power, that is, in the electric field.

Oscillations in the kHz range have been reported in the past, studied and coined as "breathing" mode oscillations [4]. In our case it was shown in a paper already published [11], featuring time-resolved measurements that a similar mechanism occurs. First, because of high ionization neutral density is depleted in the channel, greatly decreasing electron conductivity near the anode. Ions will be extracted with lower and lower energies as the gradually the potential drop moves back to the second magnetic barrier where the anode is located. At this point no ions are extracted. Then electron conductivity close to the anode increases and the electric field moves to the first magnetic barrier and the measured IEDF shift to a higher energy, closer to the total applied voltage. Ionization rate increases drastically, initiating neutral depletion and restarting the cycle. We see then in Figures 10 and 13 that distributions become single peaked upon application of sufficiently high coupled RF power. This suggests that if we allow the ID-HALL's ionization stage to govern ionization in the ionization stage, electron conductivity will remain high close to the anode, keeping the oscillations from happening, yielding a single peak distribution.

4. Conclusions

The work presented in this document has been a preliminary approach to the characterization of the ID-HALL. Our results show that it is possible to increase applied power to the ID-HALL's plasma discharge without significantly affecting specific impulse which is congruent with the concept of a working DSHT. We were also able to run the thruster at lower operating powers than if we were to otherwise run it without the activation of the FMICP source.

The average energy of the beam was also shown to approach the applied accelerating voltage, a result that corroborates the simulations of [10]. What is happening then is that the higher plasma densities achieved in the ionization stage significantly increase electron conductivity, depleting the potential step in that region. The entirety of the step arises hence in the acceleration stage, downstream from the plasma bulk.

An interesting and unexpected result was the possibility to inhibit breathing mode oscillations with the application of specific, relatively low ionization stage powers as it was seen in figures 15 and 16. In these cases, the increased electron conductivity near the anode powered by the high plasma density of the ICP source keeps the "breathing" oscillations from occurring [11]. This way discharge current oscillations disappear and the observed distributions become single peaked.

The results attained in this work look promising in the pursuit of the DSHT concept. Only half the control parameters were tested here, though. To make it conclusive, the effect of the mass flow in output current and exhaust speed will have to be evaluated.

As mentioned before, this document reports the initial phase of a much larger effort to characterize the ID-HALL thruster. Data taken during the course of this work motivated time resolved measurements that resulted a the conference paper [11] published late 2018.

References

[1] J. Arancibia Monreal, P. Chabert, and V. Godyak. Reduced electron temperature in a magnetized inductively-coupled plasma with internal coil. *Physics of Plasmas*, 20(10):103504, 2013.

[2] B. Arhipov. Development and application of electric thrusters at edb'fakel'. In *IAF, International Astronautical Congress, 50 th, Amsterdam, Netherlands*, 1999.

[3] J.-P. Boeuf. Tutorial: Physics and modeling of hall thrusters. *Journal of Applied Physics*, 121(1):011101, 2017.

[4] J. P. Boeuf and L. Garrigues. Low frequency oscillations in a stationary plasma thruster. *Journal of Applied Physics*, 84(7):3541–3554, 1998.

[5] C. Boniface, S. Mazouffre, L. Dubois, F. Gaboriau, L. Liard, D. Harribey, C. Henaux, and J. P. Boeuf. Ion acceleration through a magnetic barrier toward an optimized double-stage hall thruster concept. In *The 35th International Electric Propulsion Conference, Georgia Institute of Technology*, Oct. 2017.

[6] D. L. Brown and A. D. Gallimore. Evaluation of plume divergence and facility effects on far-field faraday probe current density profiles. Technical report, AIR FORCE RESEARCH LAB

EDWARDS AFB CA PROPULSION DIRECTORATE, 2009.

[7] A. I. Bugrova, A.V.Desyatskov, V.K.Kharchevnikov, A.S.Lipatov, and S.Zurbach. Two-modes operation of spt of second generation. In *The 30th International Electric Propulsion Conference, Florence, Italy*, Sept. 2007.

[8] F. F. Chen. *Introduction to plasma physics and controlled fusion*, volume 1. Springer, 1984.

[9] L. Dubois, F. Gaboriau, L. Liard, C. Boniface, and J. P. Boeuf. Id-hall, a new double stage hall thruster design. ii. experimental characterization of the inductive ionization source. *Physics of Plasmas*, 25(9):093504, 2018.

[10] L. Dubois, F. Gaboriau, L. Liard, D. Harribey, C. Henaux, L. Garrigues, G. J. H. Hagelaar, S. Mazouffre, C. Boniface, J. P. Boeuf, and et al. Id-hall, a new double stage hall thruster design. i. principle and hybrid model of id-hall. *Physics of Plasmas*, 25(9):093503, 2018.

[11] F. Gaboriau, L. Dubois, A. Guglielmi, J.-P. Boeuf, and G. Team. Experimental characterization of a new design of double stage hall thruster, id-hall: relevance of the concept. In *APS Meeting Abstracts*, 2018.

[12] L. Garrigues, C. Boniface, G. J. M. Hagelaar, and J. P. Boeuf. Modeling of an advanced concept of a double stage hall effect thruster. *Physics of Plasmas*, 15(11):113502, 2008.

[13] D. M. Goebel and I. Katz. *Fundamentals of electric propulsion: ion and hall thrusters*. Wiley, 2008.

[14] V. Kim, K. Kozubsky, V. Murashko, and A. Semenkin. History of the hall thrusters development in ussr. In *Proceedings of the 30th International Electric Propulsion Conference, Florence, Italy*, pages 17–20, 2007.

[15] H. Kuwano, A. Ohno, H. Kuninaka, and H. Nakashima. Development and thrust performance of a microwave discharge hall thruster. In *The 30th International Electric Propulsion Conference, Georgia Institute of Technology*, Sept. 2007.

[16] LAPLACE. Hallis, 2018.

[17] R. A. Martinez, W. A. Hoskins, P. Y. Peterson, and D. Massey. Development status of the helicon hall thruster. In *The 31th International Electric Propulsion Conference, University of Michigan, USA*, Sept. 2009.

[18] A. Morozov. *Investigation of the stationary electromagnetic plasma acceleration*. PhD thesis, Doctoral Thesis, Institute of Atomic Energy named after I.V. Kourchatov, 1965.

[19] A. I. Morozov and V. V. Savel'ev. On galateas — magnetic traps with plasma-embedded conductors. *Physics-Uspekhi*, 41(11):1049–1089, nov 1998.

[20] J. Perez-Luna, G. J. M. Hagelaar, L. Garrigues, and J. P. Boeuf. Model analysis of a double-stage hall effect thruster with double-peaked magnetic field and intermediate electrode. *Physics of Plasmas*, 14(11):113502, 2007.

[21] P. Y. Peterson and A. D. Gallimore. The performance and plume characterization of a laboratory gridless ion thruster with closed electron drift acceleration. In *40th AIAA/ASME/SAE/ASEE Joint Propulsion Conference and Exhibit*, July 2004.

[22] C. Philippe Kadlec. *Caracterisations spatio-temporelles de jets ioniques : developpement des diagnostics et application a la propulsion ionique*. PhD thesis, Universit d'Orlans, 1998. Thse de doctorat dirige par Bouchoule, Andr Physique Orlans 1998.

[23] J. SERCEL. Electron-cyclotron-resonance (ecr) plasma thruster research. In *24th Joint Propulsion Conference*, page 2916, 1988.

[24] A. Shabshelowitz, A. D. Gallimore, and P. Y. Peterson. Performance of a helicon hall thruster operating with xenon, argon, and nitrogen. *Journal of Propulsion and Power*, 30(3):664–671, 2014.

[25] S.-H. Song, Y. Yang, P. Chabert, and M. J. Kushner. Electron energy distributions in a magnetized inductively coupled plasma. *Physics of Plasmas*, 21(9):093512, 2014.